UC Berkeley
UC Berkeley Previously Published Works

Title

A flow disturbance estimation and rejection strategy for multirotors with round-trip trajectories

Permalink

https://escholarship.org/uc/item/4wd9t3bs

Authors

Byun, Jaeseung
Mäkiharju, Simo A
Mueller, Mark W

Publication Date

2020-03-05

Peer reviewed

A flow disturbance estimation and rejection strategy of multirotors with round trip trajectories

Jaeseung Byun[1], Simo A. Mäkiharju[2], and Mark W. Mueller[1]

Abstract— **This paper presents a round trip strategy of multirotors with unknown flow disturbances. The method is designed to decrease flight time for return trips, while the safety is ensured. The disturbance force and torque estimation model is derived from the onboard inertial measurement unit (IMU) sensor data. The estimation made during the previous time step is used as feedforward thrust and torque during the inbound trip, and the disturbances are recorded for the feedforward inputs of the return trip. As a demonstration of the capabilities for this approach, static point and repetitive trajectory experiments are shown along with a comparison against a conventional PD controller. The benefits of this round trip strategy is further verified by multiple experiments. Faster return trip velocity is obtained with small position errors. We also confirm drastically reduced position errors along the flow direction.[1]**

I. INTRODUCTION

Multirotors are widely used in the urban areas. Initially utilized as a new paradigm in the field of photography [1], usage of these vehicles has been extending to entertainment [2], [3], cleaning windows and solar cells [4], and inspection of urban areas [5]. Among many other possible usages, delivery is one of the most practical applications, not only as a future of package delivery system [6], but also as a present solution, such as blood delivery [7]. Despite its many characteristic capabilities (such as hovering and agility), unpredictable wind disturbances often jeopardize the reliability of the flight mission.

Majority of such practical flight missions that were previously mentioned are usually round-trips, which include an inbound trip and a returning trip. In terms of proactively readjusting itself with respect to wind flows, the information regarding the flows are nonexistant during the inbound flight. Thus, it is difficult to pursue further improvements in this case. On the other hand, it is possible to say that we have some idea on how the flow during the return flight will look like, by reflecting the experience the vehicle had during the previous flight. Once the wind information becomes available, the vehicle is able to return faster with assured safety, which improves overall productivity of the flight.

Identification and rejection of external disturbances, including wind disturbances, has been extensively studied. IMU based estimation is the most common method. Integral sliding mode control with a purely IMU-based disturbance observer was shown in [8], and was verified through a series of simulations and experiments. Although the slide controller showed the best performance during the simulation, there was no significant improvement compared to the experimental results that were obtained using a PID controller. This estimation method was extended in [9], which used momentum based integration to estimate the torque of quadrotors. This method was designed to filter undesired noise arising from the numerical differentiation of the rate gyro data. High pass filtered force estimates were applied to detect collision. The estimation of downwash effects of quadrotors using IMU sensors were first suggested in [10]. Their results verified previous theoretical models based on theoretical fluid mechanics, that gave an estimate of such effects.

Another approach for disturbance estimation is sensor fusion between IMU and other sensors. GPS-velocity data and IMU data can be incorporated via extended Kalman filtering (EKF) for wind speed estimation. The reliability of this approach was verified with ground truth wind velocity by [11]. In this study, notable assumptions were made. First, multiple drag coefficients are required a-priori. Second, Coriolis term in the angular momentum equation was neglected. An interesting approach is sensing the wind using vision sensors. Visual-inertial fusion method, which estimates direction of the vehicle and wind velocity with sensor fusion of IMU and monocular camera, is shown in [12].

Attempts in designing novel hardware that can accomplish disturbance rejection has also been under consideration by various researchers. A pressure based velocity sensor was fabricated and implemented in the quadcopter by [13], and the directly measured velocity data are plugged in to the geometric controller in [14] to ensure stability under unsteady wind conditions. An angular momentum wheel design, which makes the quadcopter resilient especially for torque disturbances, was shown in [15].

In [16], an incremental nonlinear dynamic inversion method was compared to a conventional PID controller, and showed superior performance in terms of tracking error. The accelerometer was used not only for disturbance estimation but also for control forces. The suggested rejection was experimentally validated using an open jet facility. In recently, a nonlinear model predictive control (MPC) was implemented by [17]. For the disturbance estimation, an extended Kalman filter and an unscented Kalman filter were both applied. The measurement step was updated using an onboard state estimator. Although the result showed exceptional rejection performance in terms of position errors, it was unclear how

The authors are with [1]High Performance Robotics Lab and [2]FLOW Lab, Mech. Eng. Dept., University of California, Berkeley, CA 94720, USA. {jaeseungbyun, makiharju, mwm}@berkeley.edu
[1]Experimental validation video can be found here: https://youtu.be/Re4MLd_BsL8
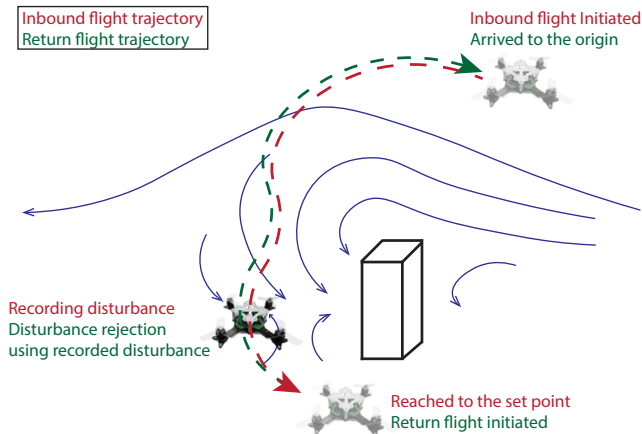
Fig. 1: Flow rejection strategy for round trip flights. The disturbances are recording during the inbound flight (red), and the gathered information is used for feedforward of the return flight (green)

the performance how the performance would be varied by the speed of the vehicle.

We present a novel round trip disturbance rejection strategy as described in Fig. 1. We assume that the entire flight is composed of five stages;

1) Inbound flight is initiated
2) During the inbound flight, estimates regarding the position of the vehicle and external disturbances are recorded using the IMU based disturbance model.
3) Once the vehicle reaches its target point, a task is conducted. Return flight is initiated.
4) In the middle of the flight, the recorded disturbances are used as a set of feedforward thrusts and torque inputs to the controller, while current estimations are also being updated. This enables improved disturbance rejection performance. Also this allows the vehicle to return with a faster velocity without experiencing any instabilities or crashing.
5) the vehicle arrived at the origin, and a new flight is initiated as necessary.

This paper is organized as follows: The disturbance estimation model is derived in II. The round trip disturbance rejection algorithm is explained in III. Experimental validation is conducted in IV. A conclusion to our work is made and future work is suggested in V

II. DISTURBANCE ESTIMATION MODEL

In this section, we introduce a disturbance estimation model for external forces and torque for a quadrotor. The model employs the data collected from an accelerometer and rate-gyro sensor data from the IMU, and the propeller thrust and torque is calculated from the control loop. We use the earth local frame as an inertial frame, while the body frame is aligned to the mass center.

A. Disturbance force estimation model

The disturbance force $\underline{f}_d$ can be derived from Newton's second law,

$$m^B \underline{a}_B^E = \sum_{i=1}^{4} \underline{f}_i + \underline{f}_d + m^B \underline{g} \tag{1}$$

where $\underline{f}_i$ is the force produced from each propeller, m^B is mass of the body, $\underline{a}_B^E$ is the linear acceleration, and $\underline{g}$ is gravitational acceleration. Here we assume that the disturbance forces acts on the mass center of the body, and the mass center is aligned with the geometric center. Accelerometer readings $\underline{\alpha}$, can be represented as a difference between the linear acceleration and gravity,

$$\underline{\alpha} = \underline{a}_B^E - \underline{g} \tag{2}$$

then (1) becomes

$$\underline{f}_d = m^B \underline{\alpha} - \sum_{i=1}^{4} \underline{f}_i \tag{3}$$

Assuming the motor force produced from the command thrust is the same as the true force produced by the propellers (i.e. secondary effects such as blade flapping [18] are not considered), then (3) becomes

$$\underline{f}_d = m^B \underline{\alpha} - c_\Sigma \underline{3}^B \tag{4}$$

where c_Σ denotes the sum of the motor forces. When the vehicle under consideration is flying, the accelerometer experiences significant vibrations, in addition to the default sensor noise. Therefore, we propose a force estimator of form,

$$\underline{f}_d = \mathcal{F}\left(\underline{f}_{d,exp}\right), \quad \underline{f}_{d,exp} = m^B \hat{\underline{\alpha}} - c_\Sigma \underline{3}^B \tag{5}$$

where $\mathcal{F}\left(\cdot\right)$ is a low-pass filter operation, and $\underline{f}_{d,exp}$ is the estimated disturbance force from the noisy accelerometer $\hat{\underline{\alpha}}$. We choose a second order filter expressed in the discreted time domain

$$\begin{aligned} \mathcal{F}\left(\underline{f}_{d,exp}[k]\right) = {} & b_0 \underline{f}_{d,exp}[k] + b_1 \underline{f}_{d,exp}[k-1] \\ & + b_2 \underline{f}_{d,exp}[k-2] - a_1 \underline{f}_d[k-1] \\ & - a_2 \underline{f}_d[k-2] \end{aligned} \tag{6}$$

where a_i and b_i are filter coefficients depending on the sampling time and cutoff frequency.

B. Disturbance torque estimation model

The total torque acting on the quadcopter $\underline{n}_B$ is given by Euler's law,

$$\underline{n}_B = D^B\left(J_B^B \underline{\omega}^{BE}\right) + \underline{\Omega}^{BE} J_B^B \underline{\omega}^{BE} \tag{7}$$

where J_B^B represents mass moment of inertia (MMOI), and $\underline{\omega}^{BE}$ is the angular velocity. Note that $\underline{\Omega}^{BE}$ is skew-symmetric form of the angular velocity vector. Total torque is composed of the disturbance torque $\underline{n}_d$ and the torque produced from the collection of propellers $\underline{n}_p$. Also, under

the assumption that we have a perfect rate-gyro sensor, $\gamma = \underline{\omega}^{BE}$, equation (7) becomes

$$\underline{n_d} = J_B^B \frac{d}{dt}\underline{\gamma} + \underline{\Gamma} J_B^B \underline{\gamma} - \underline{n_p} \tag{8}$$

Since data regarding angular acceleration are not accessible in our system, forward Euler method is applied to the rate-gyro estimation as a numerical approximation. Applying a similar procedure to (5) and (6),

$$\underline{n_d} = \mathcal{F}\left(\underline{n}_{d,exp}\right), \ \underline{n}_{d,exp} = J_B^B \frac{d}{dt}\underline{\hat{\gamma}} + \underline{\hat{\Gamma}} J_B^B \underline{\hat{\gamma}} - \underline{n_p} \tag{9}$$

III. ROUND TRIP DISTURBANCE REJECTION ALGORITHM

This section describes the detailed algorithm for round trip disturbance rejection. Fig. 1 describes a round trip trajectory for a multirotor with an unknown flow disturbance. The trajectory is composed of an inbound trajectory and return trajectory. Trips are designed to share same positions along the trajectory except for the velocity direction being reversed.

A. Controller

A cascade PD position and attitude controller were utilized as depicted in Fig. 2. Both controllers were performed offboard, while the total torque is calculated onboard. A nonlinear controller, which prioritizes yaw angle being matched with the desired yaw angle [19] is used in attitude control.
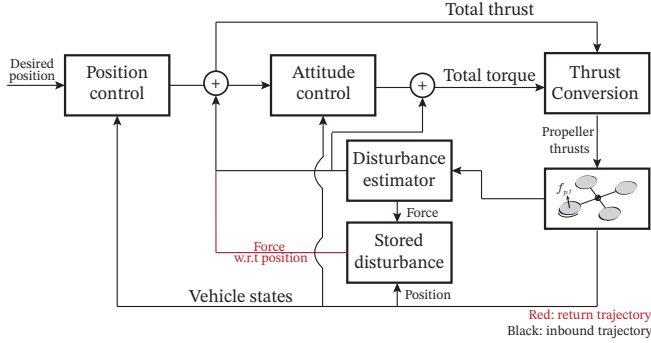

Fig. 2: Block diagram of the controller in the round trip strategy. Red arrow is used for the return flight

B. Inbound flight strategy

When the vehicle is making an inbound flight, the vehicle state is continuously updated via the disturbance estimators developed from II. Feedforward control is applied to the total thrust and torque. It is important to note that the inbound rejection algorithm must provide quality estimates so that minimum position error can be ensured. Thus, we limit the speed of the vehicle for the most accurate trajectory. At the same time, we 'record' the estimated torque and force as a function of the current position. The position is estimated offboard, meaning some data can be lost when the onboard data (total torque) are being transmitted during the recording process.

Fig. 3: The quadcopter used in the experiments

TABLE I: Physical parameters of the test vehicle

Prop. diameter (mm)	50.8
Arm length (mm)	58.5
Mass (g)	154
Maximum thrust (N)	4.6

C. Return flight strategy

The estimation and feedforward method are the same as the inbound flight, except that the trajectory is now reversed. The major difference is that we now conduct feedforward with 'recorded' data, with respect to the current position. The closest distance between the current position and the position of inbound trip trajectory is found from searching algorithm, and recorded disturbance force ($f_{d,inb}$) and torque at that particular position are extracted for rejecting disturbances.

The recorded disturbances are also used to improve our position estimator. The updated force estimate $f_{d,update}$ is,

$$\underline{f}_{d,update}[k] = \mathcal{F}\left(\underline{f}_{d,exp}[k-1] - \underline{f}_{d,inb}[k]\right) + \underline{f}_{d,inb}[k] \tag{10}$$

and we can achieve the position update by integration of the acceleration term deduced from the force update. A notable distinction from the inbound flight is that we now use wind disturbance a-priori. This not only enables us to ensure the vehicle is able to follow an accurate trajectory since disturbance of current time step is available, but also allows the vehicle to return faster with similar positional errors to that of inbound flight.

IV. EXPERIMENTAL VALIDATION

Experiments were carried out for validation; Our main interest lies in cases involving repetitive trajectories, especially the round trip scenario. The position error, attitude error, disturbance force, and disturbance torque are shown with respect to the flight time, and noticeable observations from the experimental results will be discussed.

A. Laboratory setup

The quadcopter for our demonstration and its physical parameters are described in Fig. 3 and Table I. Localization is based on a motion-capture system, complemented with the
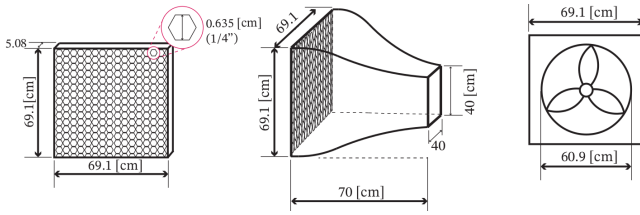
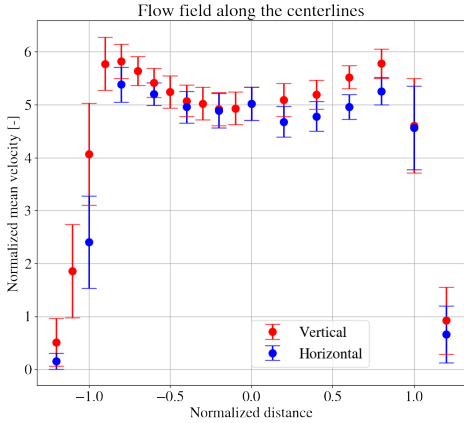Fig. 4: Dimensions for the test facility

Fig. 5: Flow field identification, $30\,\mathrm{cm}$ far from the nozzle exit. The velocity is normalized by the largest quadcopter speed in the experiment ($1\,\mathrm{m/s}$). The distance is normalized by the half edge of the nozzle ($20\,\mathrm{cm}$). Error bar denotes standard deviation of the measured velocity

rate gyro measurement. Frequency of the radio command signal is $50\,\mathrm{Hz}$. Since the total thrust is computed offboard, and the disturbance force for the return flight is also recorded with $50\,\mathrm{Hz}$. Total torque, on the other hand, is calculated onboard, which enables feedforward of the torque with frequency of $500\,\mathrm{Hz}$. The position is available with $50\,\mathrm{Hz}$, while the disturbance torque is recorded at the same frequency.

Up to $6\,\mathrm{m/s}$ of wind velocity can be imposed on the quadcopter $30\,\mathrm{cm}$ far from the nozzle exit. A constant temperature anemometer (TSI Inc. model 1212-60) when the vehicle was utilized for the velocity measurement, and an analog control circuit (TSI Inc. model 1051-2, 1054A, and 1056) with a digital converter with sampling frequency of $1000\,\mathrm{Hz}$. The detailed flow profile is given in Fig. 5, and specific dimensions are shown in Fig. 4. An accurate measure of the positions shown in the flow field was achieved by the motion-capture system.

B. Disturbance rejection performance

As discussed in III-B, more accurate position error estimates during the inbound flight allow better overall flight performance. In order to verify the accuracy of the disturbance estimator, we allow the vehicle to statically at hover at the middle of the flow field (Fig. 6).

It is unclear that whether the performance at a static flight can be extended to a flight with trajectories. For that reason, a straight-line trajectory is proposed. As shown in Fig. 6, the trajectory is designed to move the vehicle back and forth between two points. The midpoint of the straight-line is
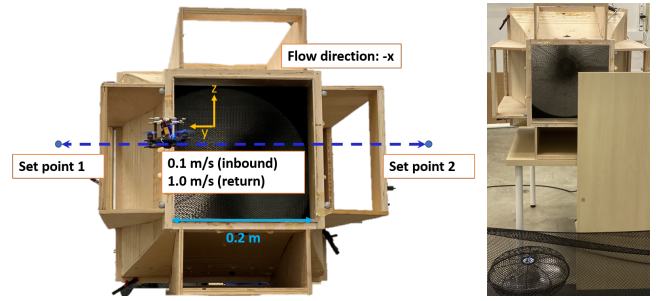

Fig. 6: Description of straight-line trajectory (left) and random flow field set-up (right)
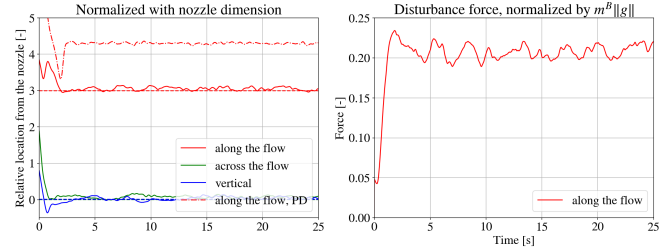

Fig. 7: Static point experiments. The distance is normalized with the nozzle dimension ($20\,\mathrm{cm}$), and the force is normalized with the weight of the vehicle

aligned with the geometric center of the nozzle. A maximum velocity of $0.1\,\mathrm{m/s}$ was chosen, since it allows us to make accurate error estimates. Repeated traversal on this trajectory was made in order to confirm that there is no directional dependence.

C. Round trip experiment with feedforward of inbound flight disturbance data. The distance is normalized with the nozzle dimension ($20\,\mathrm{cm}$), and the force is normalized with the weight of the vehicle

1) A straight-line trajectory: We finally test the performance of the new disturbance rejection strategy. Detailed explanation can be revisited in III. For the purpose of this performance test, we use two straight-line trajectory flights, while the vehicle is flying back at 10 times larger than that
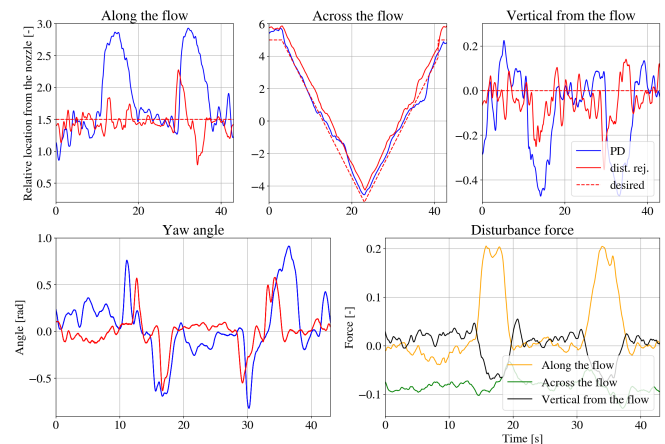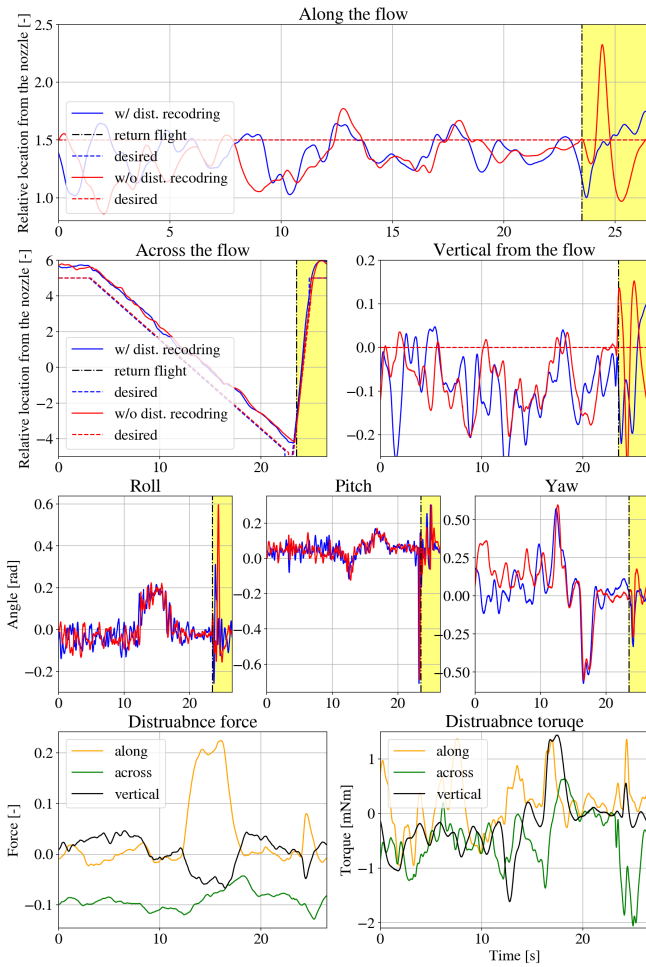

Fig. 8: Repetitive trajectory experiment

Fig. 9: Round trip straight-line trajectory experiment with velocity $1\,\mathrm{m/s}$. The distance is normalized with the nozzle dimension ($20\,\mathrm{cm}$), and the force is normalized with the weight of the vehicle

Fig. 10: Trajectory experiment with a random flow field. Return velocity of $0.5\,\mathrm{m/s}$ was chosen

of the inbound flight. Here we chose velocity of $1.0\,\mathrm{m/s}$, to check the consistency of suggested algorithm.

2) A trajectory with a random flow field: The performance of the algorithm was evaluated with a known flow field. In order to test a more realistic case, a random flow field was designed as shown in Fig. 6. A quadrant of the nozzle exit was blocked by an obstacle, and an additional fan was installed on the floor. The produced flow points upwards, and mixes with the flow from the nozzle to create a disturbance situation in real-life.

D. Results and discussion

Position and force estimation of the vehicle with a static flow field is shown in Fig. 7. As one can observe, very small position errors were achieved overall, which implies that we can accurately reject the flow at a static situation. As expected, a steady state error estimation of a conventional PD controller caused very high position error. Fig. 8 depicts position, yaw angle, and estimated disturbance force during the repetitive flight. Since the vehicle is moving across the flow, the disturbance force from the flow mainly acts along the flow direction. For this reason, similar position error
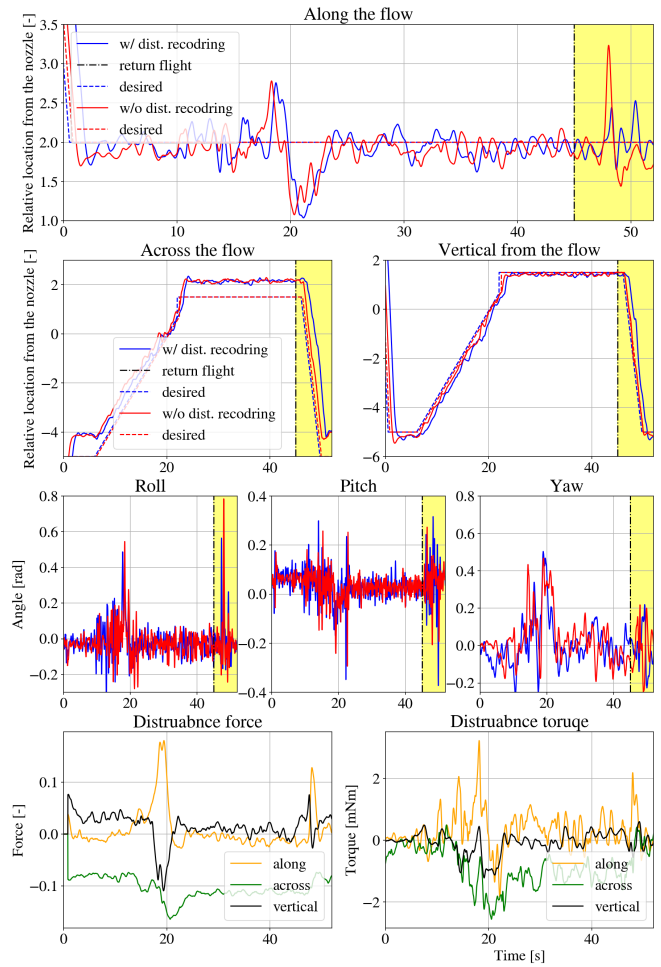
was observed compared to that of the PD controller (Fig. 7). The presence of oncoming flow also affects the flow in the vertical direction. This is because of the positive drag generated by the positive pitch angle of the vehicle flying forwards [20]. Significant yawing motion was observed near the boundary of the flow. This is due to the large velocity gradient at the boundary increases drag force only for half of the propellers, producing additional yaw torque.

Position, attitude, and complete disturbance estimation of the round trip experiment with a straight-line trajectory is given in Fig. 9. The yellow shaded area denotes the return trajectory with a velocity ten times higher than that of the inbound trip ($0.1\,\mathrm{m/s}$). The positional errors along the flow direction and the vertical flow direction were improved noticeably. In particular, a large overshoot of roll and pitch angle disappeared from the disturbance recording.

Overall, we observe that despite the introduction of the random flow field for the round trip scenario, which is described in 10, the position error remained small. The case where the recorded disturbance data were not utilized performed the worse. This indicates that the recording strategy can provide resilient counteraction for the given flow field,

even with unknown flow disturbance.

An interesting observation that can be made is that the disturbance force was underestimated by half during the return flight. This can be due to the fact that velocity of the vehicle become too fast to accurately capture the disturbance force.

V. Conclusions

In this paper, a simple and novel disturbance rejection algorithm specializing in round trip trajectory for multirotors have been introduced. The key idea is to record disturbances as a function of position for the inbound flight, and retrieve the recorded disturbances to the controller and estimation update part during the return flight.

Performance in the sense of minimizing position error and attitude error was verified with static and dynamic experiments, and was compared in a conventional cascade PD controller. The results were in accord with our current understandings.

Finally, a series of experiments covering a round trip scenario was conducted with our suggested algorithm. The return flight showed improved position error, even compared to the position error of the inbound flight, even for the case where the vehicle speed was increased tenfold. Also, our algorithm did not deteriorate when subjected to the trip scenario with a straight-line trajectory with unknown flow disturbances.

Acknowledgment

References

[1] M. Germen, "Alternative cityscape visualisation: drone shooting as a new dimension in urban photography," *Electronic visualisation and the arts*, pp. 150–157, 2016.

[2] A. Schöllig, F. Augugliaro, S. Lupashin, and R. D'Andrea, "Synchronizing the motion of a quadrocopter to music," in *2010 IEEE International Conference on Robotics and Automation*. IEEE, 2010, pp. 3355–3360.

[3] H. Kim and J. A. Landay, "Aeroquake: Drone augmented dance," in *Proceedings of the 2018 Designing Interactive Systems Conference*, ser. DIS 18. Association for Computing Machinery, 2018.

[4] M. Hassanalian and A. Abdelkefi, "Classifications, applications, and design challenges of drones: A review," *Progress in Aerospace Sciences*, vol. 91, pp. 99–131, 2017.

[5] R. L. Mota, L. F. Felizardo, E. H. Shiguemori, A. C. Ramos, and F. Mora-Camino, "Expanding small uav capabilities with ann: a case study for urban areas inspection," *British Journal of Applied Science & Technology*, vol. 4, no. 2, p. 387, 2014.

[6] R. D'Andrea, "Guest editorial can drones deliver?" *IEEE Transactions on Automation Science and Engineering*, vol. 11, no. 3, pp. 647–648, 2014.

[7] E. Ackerman and M. Koziol, "The blood is here: Zipline's medical delivery drones are changing the game in rwanda," *IEEE Spectrum*, vol. 56, no. 5, pp. 24–31, 2019.

[8] T. Tomić, "Evaluation of acceleration-based disturbance observation for multicopter control," in *2014 European Control Conference (ECC)*. IEEE, 2014, pp. 2937–2944.

[9] T. Tomić, C. Ott, and S. Haddadin, "External wrench estimation, collision detection, and reflex reaction for flying robots," *IEEE Transactions on Robotics*, vol. 33, no. 6, pp. 1467–1482, 2017.

[10] K. P. Jain, T. Fortmuller, J. Byun, S. A. Mäkiharju, and M. W. Mueller, "Modeling of aerodynamic disturbances for proximity flight of multirotors," in *2019 International Conference on Unmanned Aircraft Systems (ICUAS)*. IEEE, 2019, pp. 1261–1269.

[11] L. Sikkel, G. de Croon, C. De Wagter, and Q. Chu, "A novel online model-based wind estimation approach for quadrotor micro air vehicles using low cost mems imus," in *2016 IEEE/RSJ International Conference on Intelligent Robots and Systems (IROS)*. IEEE, 2016, pp. 2141–2146.

[12] D. Abeywardena, Z. Wang, G. Dissanayake, S. L. Waslander, and S. Kodagoda, "Model-aided state estimation for quadrotor micro air vehicles amidst wind disturbances," in *2014 IEEE/RSJ International Conference on Intelligent Robots and Systems*. IEEE, 2014, pp. 4813–4818.

[13] D. Yeo, N. Sydney, D. A. Paley, and D. Sofge, "Onboard flow sensing for downwash detection and avoidance with a small quadrotor helicopter," in *AIAA Guidance, Navigation, and Control Conference*, 2015, p. 1769.

[14] W. S. Craig, D. W. Yeo, and D. A. Paley, "Geometric control of a quadrotor in wind with flow sensing and thrust constraints: Attitude and position control," in *AIAA Scitech 2019 Forum*, 2019, p. 1192.

[15] N. Bucki and M. W. Mueller, "A novel multicopter with improved torque disturbance rejection through added angular momentum," *International Journal of Intelligent Robotics and Applications*, vol. 3, no. 2, pp. 131–143, 2019.

[16] E. J. Smeur, G. C. de Croon, and Q. Chu, "Cascaded incremental nonlinear dynamic inversion for mav disturbance rejection," *Control Engineering Practice*, vol. 73, pp. 79–90, 2018.

[17] D. Hentzen, T. Stastny, R. Siegwart, and R. Brockers, "Disturbance estimation and rejection for high-precision multirotor position control," *arXiv preprint arXiv:1908.03166*, 2019.

[18] R. Mahony, V. Kumar, and P. Corke, "Multirotor aerial vehicles: Modeling, estimation, and control of quadrotor," *IEEE Robotics and Automation magazine*, vol. 19, no. 3, pp. 20–32, 2012.

[19] M. W. Mueller, "Multicopter attitude control for recovery from large disturbances," *arXiv:1802.09143*, 2018.

[20] R. Gill and R. D'Andrea, "Propeller thrust and drag in forward flight," in *2017 IEEE Conference on Control Technology and Applications (CCTA)*. IEEE, 2017, pp. 73–79.